catalysts

MDPI

Article

Photocatalytic Degradation of Diazinon with a 2D/3D Nanocomposite of Black Phosphorus/Metal Organic Framework

Philani V. Hlophe and Langelihle N. Dlamini *

Department of Chemical Sciences, Doornfontein Campus, University of Johannesburg, P.O. Box 17011, Doornfontein, Johannesburg 2028, South Africa; philanhlophe13@gmail.com
* Correspondence: lndlamini@uj.ac.za

Abstract: Metal–organic frameworks (MOFs) are promising materials for the removal and photodegradation of pesticides in water. Characteristics such as large surface area, crystalline structure and catalytic properties give MOFs an advantage over other traditional adsorbents. The application of MOFs in environmental remediation is hindered by their ability to only absorb in the UV region. Therefore, combining them with an excellent charge carrier 2D material such as black phosphorus (BP) provides an attractive composite for visible-light-driven degradation of pesticides. In the study, a nanocomposite of black phosphorus and MIL-125(Ti), defined as BpMIL, was prepared using a two-stage hydrothermal and sonication route. The as-prepared composite was characterized using transmission electron microscopy (TEM), scanning electron microscopy (SEM), X-ray diffraction (XRD), X-ray photoelectron spectroscopy (XPS), electrochemical impedance spectroscopy (EIS) and photoluminescence (PL) spectroscopy. These techniques revealed that the circular and sheet-like morphology of the nanocomposites had minimum charge recombination, allowing them to be effective photocatalysts. Furthermore, the photocatalysts exhibited extended productive utilization of the solar spectrum with inhibited recombination rate and could be applied in visible-light-driven water treatment. The photodegradation of diazinon in water was studied using a series of BpMIL (4%, 6% and 12% by mass) nanocomposites as a photocatalyst. The optimal composite was determined to be 4%BpMIL. The degradation parameters were optimized and these included photocatalyst dosage, initial diazinon concentration and pH of the solution. The optimal conditions for the removal and degradation of diazinon were: neutral pH, [diazinon] = 20 mg/L, photocatalyst dosage = 0.5 g/L, achieving 96% removal of the pesticide after 30 min with 4%BpMIL, while MIL-125(Ti) showed 40% removal. The improved photodegradation efficiency of the 4%BpMIL composite was attributed to Ti^{3+}-Ti^{4+} intervalence electron transfer and the synergistic effect between MIL-125(Ti) and BP. The photodegradation followed pseudo-first-order kinetics with a rate constant of 1.6×10^{-2} min^{-1}.

Keywords: diazinon; nanocomposite; photodegradation

Citation: Hlophe, P.V.; Dlamini, L.N. Photocatalytic Degradation of Diazinon with a 2D/3D Nanocomposite of Black Phosphorus/Metal Organic Framework. *Catalysts* **2021**, *11*, 679. https://doi.org/10.3390/catal11060679

Academic Editor: Anna Zielińska-Jurek

Received: 28 April 2021
Accepted: 18 May 2021
Published: 27 May 2021

1. Introduction

Pesticides are common contaminants found in water systems as a result of various activities such as chemical spills, industrial effluents and agricultural runoffs [1]. Organophosphorus pesticides are characterized by high toxicity plus carcinogenicity in the environment as well as humans because of their persistence and stability [2].

Diazinon (Figure 1) falls under a class of moderately hazardous pesticides which includes dichlorodiphenyltrichloroethane (DDT) and chlordane, amongst others. This group of pesticides has been categorized as potential carcinogens and classified as belonging to Group 2A by the World Health Organization (WHO) [3]. This organophosphorus pesticide demonstrates a vapor pressure of 1.4 mmHg at 200 °C and a Henry's law constant of 1.4×10^{-6} mm^3 mol^{-1} [4]. These properties indicate that diazinon is less volatile in soil and water, suggesting the persistence of this pesticide in water systems. Therefore, the removal of this pesticide should be an effective remediation method in wastewater treatment.

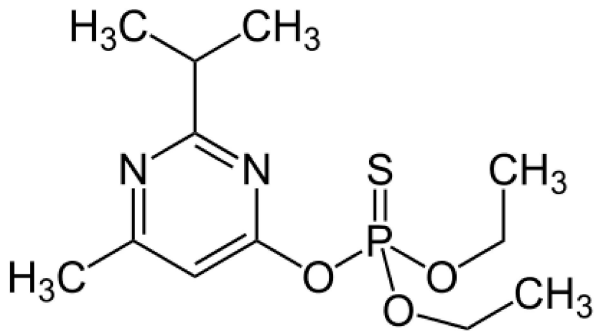

Figure 1. Structure of diazinon.

Several methods have been developed, such as adsorption, chemical coagulation, membrane technology and bioremediation. However, photocatalytic degradation of diazinon using photocatalysis has proven to be highly efficient, and leads to the production of less harmful degradation fragments [1,5,6].

Photocatalytic degradation of pesticides assisted by semiconductors such as TiO_2 has garnered massive research attention as it provides a strategy to remedy environmental pollution through the mineralization of organic pollutants into carbondioxide and inorganic anions through mineralization [7].

Traditional semiconductors such as TiO_2, WO_3 and ZnO are UV active which limits their effectual utilization of solar energy [8]. It is therefore important to fabricate visible light-oriented photocatalysts to overcome the shortcomings of UV-active materials. Nevertheless, some visible light-driven materials such as $BiVO_4$ and WO_3 suffer from electron–hole recombination, which limits their photocatalytic performance [9].

The synthesis of visible light-driven photocatalysts with effectual separation of electrons and holes through the formation of semiconductor heterojunctions, which depend on the scaffolded arrangement of the valence and conduction band positions, has been explored [10]. Heterojunction formation is the spatial separation of photogenerated charge carriers through the formation of a junction which directs electrons and holes to different materials [9]. The separation of charge carriers is propitious for photocatalysis as it allows for reduction and oxidation reactions to occur [11].

Considerable attention has been given to metal–organic frameworks (MOFs). These materials have an extended three-dimensional network and they are made up of organic linkers and metal-oxo clusters [12]. MOFs are characterized by an intriguing crystalline structure, large surface area, high pore volume and fascinating electrical, optical and catalytic properties [13]. These exceptional properties have led to the successful application of these materials in heterogeneous catalysis, gas storage and separation, sensor devices and chemical separation [14]. The drawback of these materials, however, is their limited effectual utilization of solar energy as they are only active under the ultraviolet region, which only accounts for 5% of the whole solar spectrum.

Recent research studies have explored a new photoactive titanium-based metal–organic framework, MIL-125(Ti), exhibiting $Ti_8O_8(OH)_4(BDC)_6$ BDC = 1,4-benzenedicarboxylic acid which can be used as an adsorbent for contaminants because of its relatively large surface area.

MIL-125(Ti) is a crystal clear titanium dicarboxylate exhibiting outstanding absorbance ability and encapsulation potential and good permeability, thermal strength and admirable photochemical characteristics [15]. As a result of the framework's porosity, the secondary building units (SBUs) transport reductive intermediates away from the reactive sites. This is because the material has a rigid coordination environment ideal to create chromophore sites by introducing metal co-catalysts to the SBUs. Additionally, this material is decorated with numerous inactive Ti sites [15]. However, its application in photocatalytic platforms is limited due to its activation only in the UV light region and fast charge recombination, resulting in poor photocatalytic efficiency.

It is thus necessary to design a surface-enhanced MIL-125(Ti) composite for efficient photocatalytic performance.

Wang et al. showed that MIL-125(Ti) using graphitic carbon nitride via a facile solvothermal strategy was found to exhibit excellent photoactivity for the degradation of Rhodamine B under visible light illumination [16].

Yang et al. synthesized a $BiVO_4$/MIL-125(Ti) hybrid photocatalyst via a two-step hydrothermal route and the heterojunction interface between $BiVO_4$ and MIL-125(Ti) resulted in the spatial separation of photo-induced charge carriers, which was evidenced by the high photocatalytic performance of the composite in the degradation of Rhodamine B [17].

Furthermore, Yaun et al. extended the light absorption edge of MIL-125(Ti) into the visible region by using 2-aminoterephthalic acid as the organic linker [18]. The NH_2-MIL-125(Ti) composite exhibited enhanced Cr(VI) photoreduction performance under visible light irradiation.

The limitation of MIL-125(Ti) is fast recombination of charge carriers, therefore, combination with 2D materials such as graphene or black phosphorus would mask this defect.

Black phosphorus (BP), an sp^3-bonded one atom thick two-dimensional phosphorus layer, has been receiving rave reviews for enhancing the photocatalytic activity of photocatalysts as it is an excellent charge transporter [19]. BP has a layer-dependent bandgap spanning from 0.3 eV for bulk to 2.0 eV for the monolayer intermediate [20]. This enables BP to be maximized for several applications by selecting the "right" thickness. The downside of this material, however, is its susceptibility to degradation under ambient conditions, which hinders its application.

The exploration of 2D/MOF composites for photocatalytic applications by taking advantage of the catalytic properties of MOFs and the fast carrier mobility of 2D materials is an exciting field [21,22]. However, not much work has been focused on the application of these composites in the removal of diazinon in water.

Thus, in this work, we report for the first time the synthesis of the MIL-125(Ti)/BP photocatalyst with enhanced photoactivity for the degradation of diazinon, which, to the best of our knowledge, has not been reported elsewhere. Furthermore, the optimized degradation conditions and mineralization of diazinon were investigated in the presence of UV illumination.

2. Results

Characterization of Photocatalysts

The characterization of the nanocomposites reported in this section was discussed comprehensively in our previous work [23]. Figure 2 presents that the morphology of synthesized nanocomposites as observed from SEM and TEM. More precisely, Figure 2a reveals the block orientation of MIL-125(Ti), while the sheet-like morphology of exfoliated FLBP is demonstrated in Figure 2b. The composite 4%BpMIL, which was selected as the optimum from our previous work, exhibited both sheet-like and blocked morphology, as shown in Figure 2c. The TEM pictorial illustrations presented in Figure 2d–f re-affirm the morphological findings from SEM.

The polymorphs of the nanocomposites were confirmed through XRD patterns shown in Figure 3A. The successful formation of a heterojunction was substantiated by the appearance of diffraction peaks corresponding to MIL-125(Ti) (*) and FLBP (#). The significance of heterojunction formation from the viewpoint of recombination was studied through PL and Nyquist plots presented in Figure 3B,C, respectively.

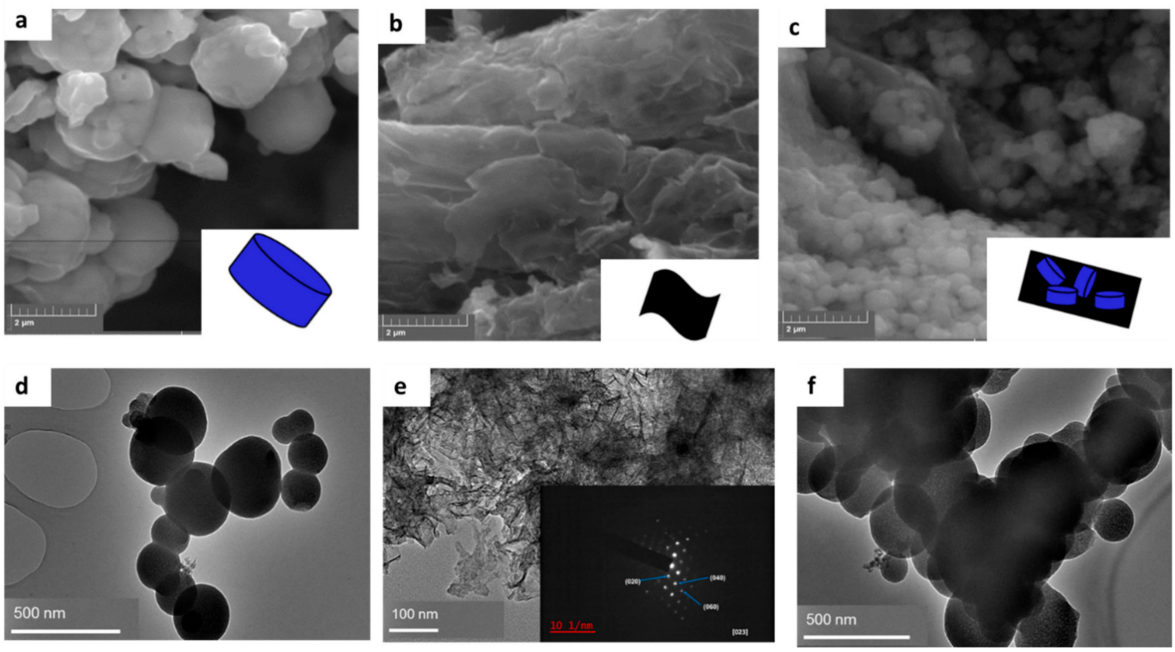

Figure 2. (**a**–**c**) Images of MIL-125(Ti), FLBP, 4%BpMIL from SEM and (**d**–**f**) images of MIL-125(Ti), FLBP, 4%BpMIL from TEM [23].

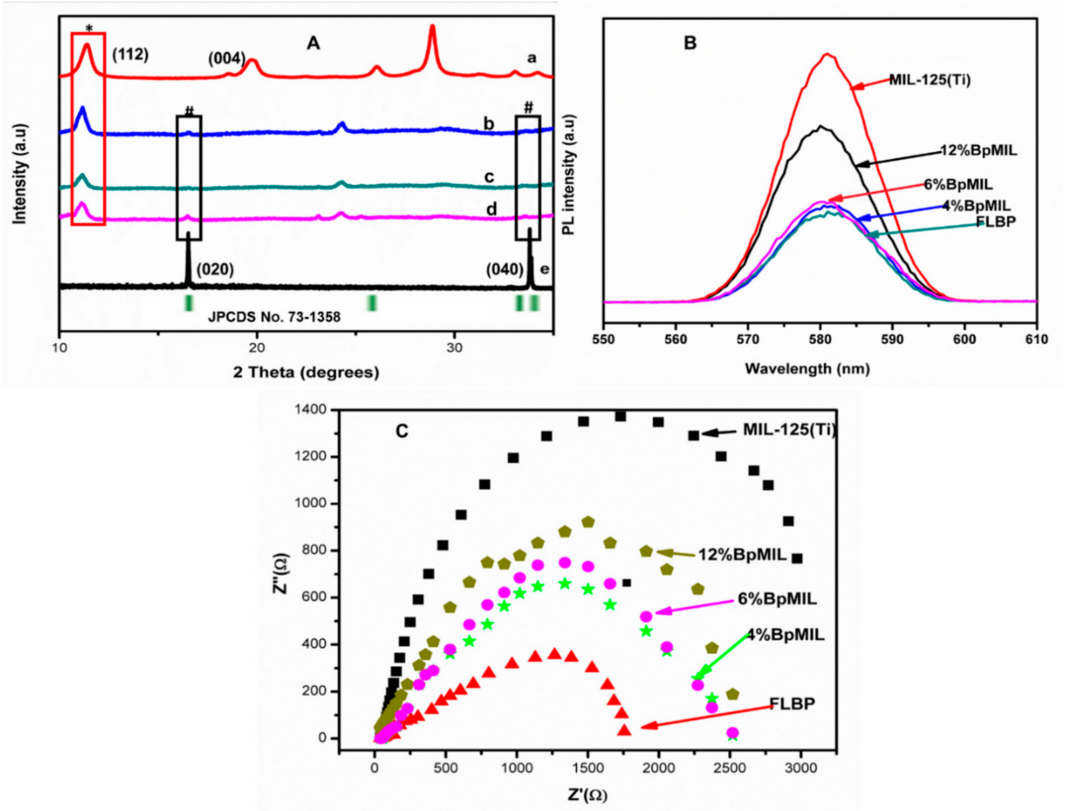

Figure 3. (**A**) XRD patterns of (a) MIL-125(Ti), (b) 4%BpMIL, (c) 6%BpMIL, (d) 12%BpMIL. (**B**) PL spectra of nanoparticles (excitation wavelength = 242 nm). (**C**) Nyquist plots of synthesized NPs [23].

The composites displayed a suppressed recombination rate compared to MIL-125(Ti), validating that heterojunction formation reduces the recombination rate.

The formation of a heterojunction as elucidated from XRD was further confirmed by the VBXPS data (Figure 4A) as a result of the red shift observed for 4%BpMIL (2.24 eV) as opposed to 1.62 eV for FLBP. The VBXPS data gave a precise numerical value of the valence band potential and, thus, 4%BpMIL showed inhibited recombination resulting from the separation of photogenerated electrons and holes.

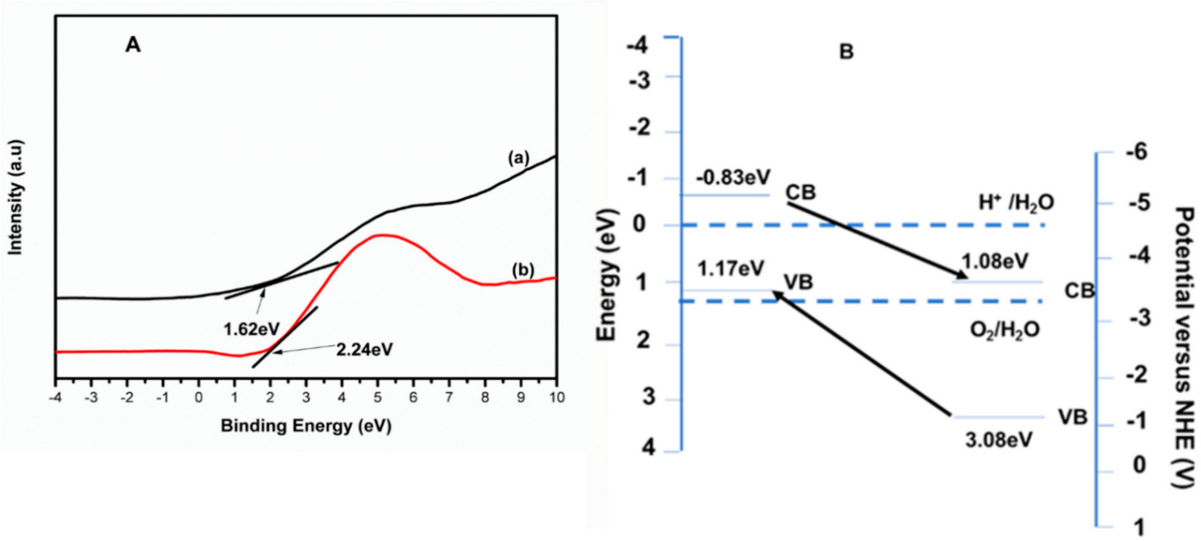

Figure 4. (**A**) The VBXPS spectra (a) FLBP and (b) 4%BpMIL. (**B**) Band positions of 4%BpMIL [23].

This was complemented by the scaffolded arrangement of the conduction and valence band potentials which were favorable for electron–hole pair separation, as depicted in Figure 4B.

The band edge potentials were computed using Equations (1) and (2)

$$E_{VB} = X - E^0 + 0.5E_g \quad (1)$$

$$E_{CB} = E_{VB} - E_g \quad (2)$$

where E_{VB}, E_{CB} are, respectively, the valence and conduction band potentials, E^0 is approximately 4.5 eV, defined as the energy of free electrons vs. normal hydrogen electrode and X is the electronegativity of the semiconductor, calculated from the geometric average of the electronegativity of elemental atoms [22]. The electronegativity of MIL-125(Ti) was computed to be 6.58 eV while that of FLBP was 4.67 eV.

The band positioning and the VBXPS data revealed that 4%BpMIL would be ideal for visible-light-driven photodegradation of diazinon in water.

The surface charges of the nanocomposites were evaluated through zeta potential studies. Figure 5 depicts the zeta potential of the photocatalysts against change in pH. The point of zero charge (pzc) of pristine MIL-125(Ti) was observed to be at pH 3.3, while the isoelectric points for the nanocomposites 4%, 6% and 12%BpMIL were found to be 3.5, 3.8 and 4, respectively. Collectively, this revealed that all the materials were negatively charged at neutral and basic pH, while they demonstrated positive surfaces in acidic pH. The pK_a value of diazinon is 2.6, from the literature [6]. On account of this value, the surface of diazinon was expected to be negatively charged above this value.

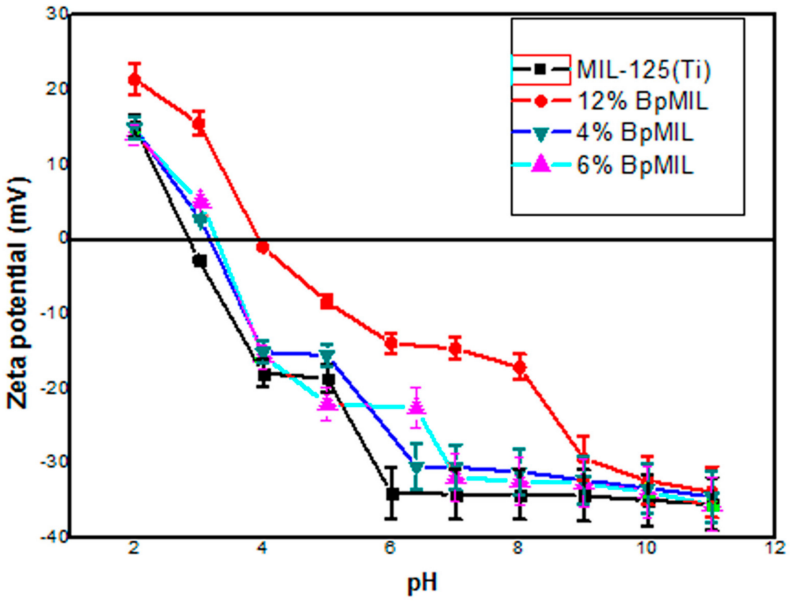

Figure 5. Zeta potentials of nanocomposites as a function of pH.

3. Discussion

3.1. Photodegradation Studies

3.1.1. Influence of Different Photocatalysts on Photodegradation of Diazinon

Figure 6 presents the photodegradation of diazinon using the various nanocomposite photocatalysts. This was evaluated by degrading 20 mg/L of diazinon at neutral pH and constant loading (0.5 g/L) of the photocatalysts. The results revealed that MIL-125(Ti) exhibited the lowest removal of diazinon (40%), while 4%BpMIL had the highest diazinon removal (95% after 30 min). The BpMIL composites showed a higher removal due to the synergistic effect between MIL-125(Ti) and BP. The high removal rate related to 4%BpMIL could be attributed to this composite possessing the lowest recombination rate and enhanced visible light activity, which was shown by the characterization studies discussed earlier. Thus, 4%BpMIL was chosen as the optimum photocatalyst for the work reported here.

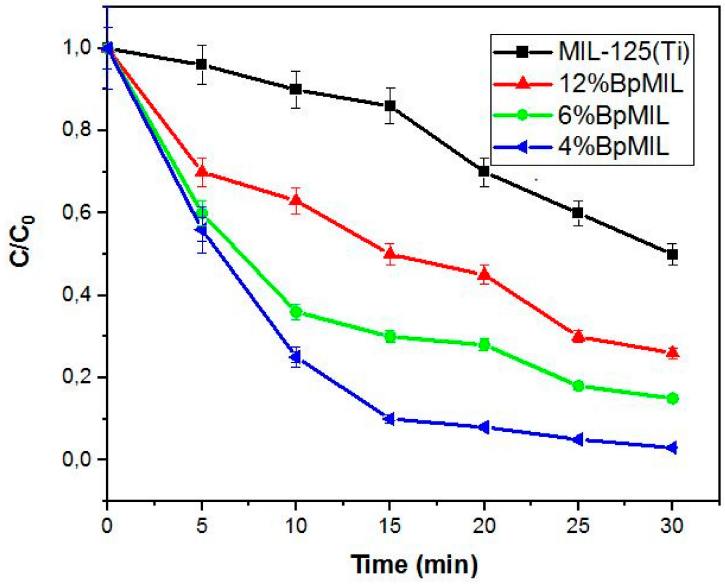

Figure 6. Degradation of diazinon (20 mg/L) using different photocatalysts at pH = 7 and nanocomposite = 0.5 g/L.

3.1.2. Influence of Initial pH on Photodegradation of Diazinon

The role of pH on the photodegradation efficiency of diazinon was evaluated in the pH range 3–11, at constant nanocomposite dosage (0.5 g/L) and constant diazinon concentration (0.5 g/L). Figure 7 shows that optimum photodegradation efficiency was observed at neutral pH. The point of zero charge (pzc) of 4%BpMIL was determined to be 3.5. The 4%BpMIL photocatalyst surface was positively charged when pzc > pH, whereas it was negatively charged when pzc < pH.

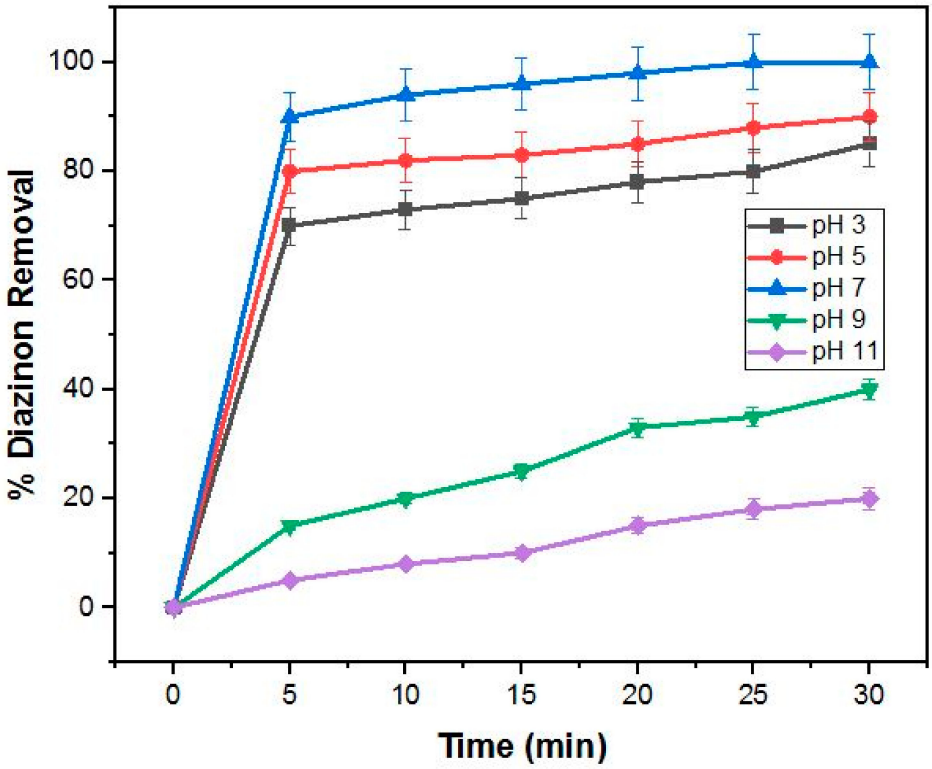

Figure 7. Degradation of diazinon (20 mg/L) using 0.5 g/L 4%BpMIL at different pH values.

The electrostatic interaction between the surface of 4%BpMIL and diazinon can be used to account for the difference in photodegradation efficiency in different pH solutions. Since the pK_a value of diazinon is 2.6, diazinon was negatively charged above this value, whereas the catalyst was positively charged below 3.5.

The corresponding ionization equations are shown in Equations (3) and (4).

$$(4\%BpMIL)\text{-}OH + H^+ \longrightarrow (4\%BpMIL)\text{-}OH_2{}^+ \ (pH < pzc) \quad (3)$$

$$(4\%BpMIL)\text{-}OH \longrightarrow (4\%BpMIL)\text{-}O^- + H^+ \ (pH > pzc) \quad (4)$$

Thus, the optimum condition could be achieved in the range pK_a (diazinon) < pH < pH_{PZC} (4%BpMIL), where the negatively charged diazinon and positively charged photocatalyst should easily attract each other, which correlates to enhanced adsorption of the pesticide onto 4%BpMIL and thus increased degradation efficiency. Neutral pH was selected for subsequent experiments to preserve the stability of the MOF material [23].

However, at alkaline pH, both materials are negatively charged and hence electrostatic repulsion between the two causes reduced adsorption of diazinon onto the nanocomposite and, therefore, results in decreased photodegradation efficiency. In this work, neutral pH was selected for optimal conditions.

3.1.3. Influence of Diazinon Concentration

The photodegradation removal of diazinon was explored by changing the concentration of diazinon (10 mg/L, 20 mg/L, 30 mg/L, 40 mg/L, 50 mg/L) at neutral pH and 0.5 g/L loading of the nanocomposite. The results are depicted in Figure 8, which reveal that the photodegradation efficiency of diazinon decreased from approximately 98% to about 80% with increasing diazinon concentration from 10–50 mg/L in 30 min. Other researchers have also reported a decrease in degradation efficiency of diazinon with an increase in diazinon concentration [5,24].

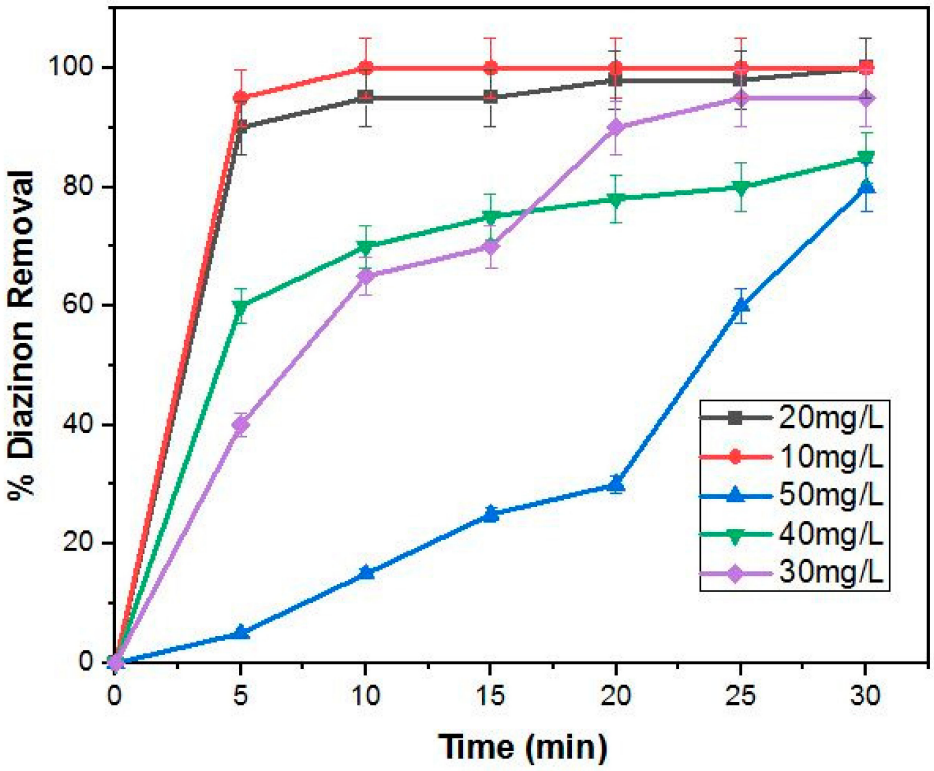

Figure 8. Degradation of different concentrations of diazinon at neutral pH and 0.5 g/L 4%BpMIL.

This decline in degradation efficiency may be ascribable to the decreased adsorption sites as a result of more adsorption of diazinon on the surface of the photocatalyst [1]. The degradation efficiency decreased with increased diazinon concentration and Jonidi-Jafari et al. [5] postulated that the photocatalyst surface adsorbs more diazinon molecules at higher concentrations of this pesticide.

3.1.4. Influence of Photocatalyst Quantity

Studies to investigate the effect of varying the 4%BpMIL photocatalyst (0.1, 0.5, 1 and 2 g/L) at pH 7 and constant diazinon concentration (20 mg/L) are presented in Figure 9. The results revealed that the removal of diazinon was approximately 98% for the 0.5 and 1 g/L loadings, however, the degradation efficiency was reduced to around 70% with the application of 2 g/L of the photocatalyst. In addition, an increase in removal efficiency was observed when the quantity of the photocatalyst was changed from 0.1–0.5 g/L. Kaneco et al. reported the mineralization of diazinon with nanosized photocatalyst TiO_2 in water under sunlight irradiation, and the removal efficiency of diazinon was 90% within 80 min. In our work, the diazinon degradation efficiency was better compared to those results [24].

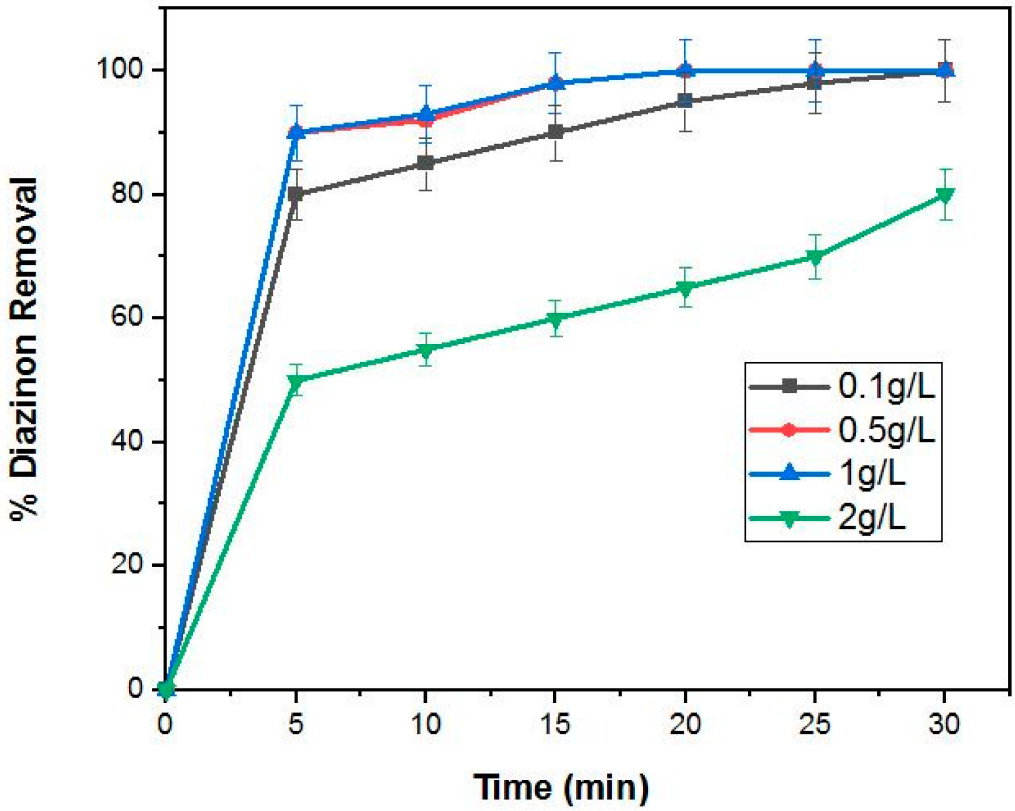

Figure 9. Degradation of diazinon concentration (20 mg/L) at pH = 7, using different photocatalyst quantities (0.1, 0.5, 1 and 2 g/L).

This increment may be attributed to more diazinon molecules being adsorbed on the surface of 4%BpMIL with an increase in photocatalyst quantity. The decrease in efficiency with an increase in catalyst dosage from 0.5–2 g/L could be explained by the occurrence of light scattering which inhibits the aggregation and performance of photocatalyst particles [5].

3.2. Degradation Kinetics

The plots of ln([diazinon]/[diazinon]$_0$) versus time for the degradation of diazinon are shown in Figure 10. The plots depict straight lines exhibiting slopes that relate to pseudo-first-order rate constants. The photodegradation of the diazinon pathway followed a pseudo-first-order mechanism.

The rate constant was deduced from the gradient of ln([diazinon]/[diazinon]$_0$) against time. The loading 0.5 g/L showed the highest rate constant of 1.6×10^{-2} min^{-1}, while the 2 g/L loading had the lowest rate constant (0.8×10^{-3} min^{-1}). The results are tabulated in Table 1.

Table 1. Reaction kinetics values for diazinon degradation.

[4%BpMIL] (gL^{-1})	K_{value} (min^{-1})	R^2
0.1	1.0×10^{-2}	0.9710
0.5	1.6×10^{-2}	0.9804
1	1.6×10^{-2}	0.9628
2	8.0×10^{-3}	0.9797

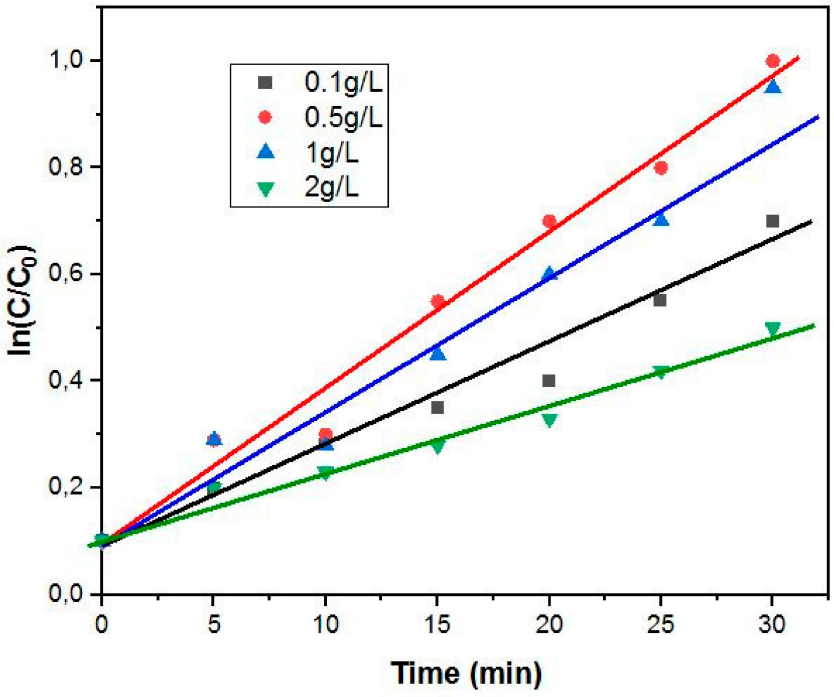

Figure 10. Photodegradation kinetics of diazinon using different concentrations of 4%BpMIL.

Figure 11 depicts a proposed mechanism for the degradation of diazinon and this is summarized by Equations (7)–(11). Hlophe et al. [23] presented that when 4%BpMIL is irradiated with UV light (λ < 365 nm), electrons are excited and transferred to the conduction band from the valence band, which generates electron–hole pairs, as shown in Equations (5) and (6).

$$\mathrm{FLBP} + hv \longrightarrow \mathrm{FLBP}\left(e^- + h^+\right) \quad (5)$$

$$\mathrm{MIL-125(Ti)} + \mathrm{e}^- \rightarrow \mathrm{Ti}^{3+} - \mathrm{MIL-125(Ti)} \quad (6)$$

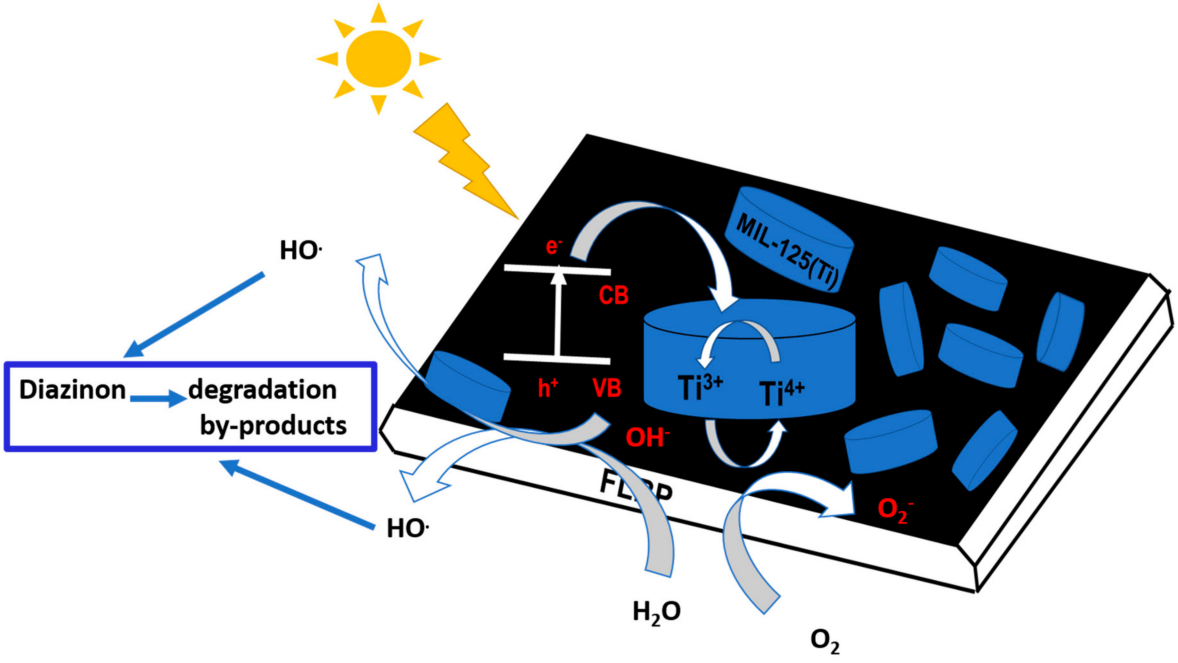

Figure 11. Schematic of diazinon degradation.

Then, reactions between electrons and O_2 occur, while positively charged holes react with H_2O or OH^- to release reactive $OH^{\cdot}$, which can oxidize diazinon and its degradation fragments [1,5].

$$Ti^{3+} - MIL - 125(Ti) + O_2 \rightarrow Ti^{4+} - MIL - 125(Ti) + O_2 \quad (7)$$

$$h^+_{VB} + \text{diazinon} \rightarrow \text{diazinon}^{\cdot +} \rightarrow \text{oxidation of diazinon} \quad (8)$$

$$h^+_{VB} + H_2O \rightarrow H^+ + OH^{\cdot} \quad (9)$$

$$h^+_{VB} + OH^- \rightarrow OH^{\cdot} \quad (10)$$

$$h^+_{VB} + \text{diazinon} \rightarrow \text{diazinon degradation} \quad (11)$$

The distribution of the reaction fragments from the photodegradation of diazinon in aqueous media through an advanced oxidation process has been presented in a previous study by Shemer et al. [25]. The investigation revealed that the sulfate ion was cleaved first, and then generation of phosphate, carbonate and nitrate ions occurred. The chemical structure of diazinon can be used to elucidate these results, as the sulfur groups could easily detach from the diazinon molecule and lose electrons to form sulfate anions. Kouloumbos et al. [24] reported similar findings.

4. Materials and Methods

4.1. Chemicals

All regents and solvents utilized were of analytical reagent grade and used as received from suppliers. Terephthalic acid (BDC), *N*′*N*-dimethylformanide (DMF), *N*-methylpyridine (NMP), sodium hydroxide (NaOH), titanium isopropoxide (TBOT), bulk black phosphorus, ethanol (≥99.8% absolute), sodium sulphate (≥99% Reagent Plus), polyvinylidene fluoride (PVDF) and methanol were purchased from Sigma-Aldrich Co. Ltd., Johannesburg, South Africa.

4.2. Synthesis of BpMIL Composites

Few layer black phosphorus (FLBP) was synthesized following methods reported in the literature [23]. The MIL-125(Ti) was fabricated according to an approach previously reported with slight adjustments [26]. The composites were prepared by varying the weight loadings of MIL-125(Ti) while keeping the amount of FLBP constant. Typically, MIL-125(Ti) (1.8×10^{-4}, 3.6×10^{-4} and 5.4×10^{-4} mol) was added to 10 mL of FLBP. This dispersion was then sonicated for 2 h, after which it was centrifuged and washed with ethanol three times. The wet powders were then dried in an oven at 60 °C overnight. The composites were denoted 4%BpMIL, 6%BpMIL and 12%BpMIL (m/m).

4.3. Theory/Calculation

4.3.1. Characterization

Work we have published elsewhere [23] shows that morphologies of the nanocomposites, having been captured using scanning electron microscopy (SEM) and transmission electron microscopy (TEM). The SEM (TESCAN Vega TC) equipped with VEGA 3 TESCAN software was operated under nitrogen gas at a working voltage of 20 kV. The SEM coupled with energy dispersive spectroscopy (EDS) was also operated at the same voltage and was used to probe the elemental composition of the nanoparticles (NPs). Furthermore, TEM was used to capture the images of the NPs at an accelerating voltage of 200 kV. Prior to analysis, the nanocomposites were sonicated in ethanol before being dropped on carbon-coated copper grids.

The polymorphs of the NPs from SAED patterns were verified utilizing powdered X-ray diffraction (X'Pert Philips) with a CuKα radiation (0.1540 nm) polychomator beam in the 2θ scan range 20–80 °C. A step size and step time of 0.0170 (2θ) and 87.63 s were used at 40 kV and 40 mA instrument power settings.

Optical properties of the nanocomposites were studied from the viewpoint of photoluminescence spectra. They were recorded using an LS 45 fluorescence spectrometer (Perkin Elmer) at a 242 nm wavelength.

The Metro Autolab:Nova 2.0 potentiostat was used to evaluate the electrochemical measurements. The potentiostat comprised a standard three-electrode system with Ag/AgCl as a reference electrode, a Pt wire as a counter electrode and a working electrode fabricated using fluorine-doped tin oxide (FTO) glass with NPs pasted on the fluorine-doped side. A mixture of polyvinylidene fluoride (PVDF) and as-prepared nanocomposites in the ratio 10:1 were added to 1 mL *N*-methylpyridine (NMP) to fabricate the working electrode. A homogeneous slurry from the combination of the nanocomposites, PVDF and NMP was decorated onto the FTO glass and left to dry at room temperature overnight. To establish a good flow of electric current to the potentiostat, a copper wire was attached utilizing silver paste which was air dried at room temperature for 24 h The electrochemical impedance spectroscopy (EIS) spectra were recorded at a frequency range of 100 kHz to 0.1 Hz at an AC voltage of 10 mV rms vs. E_{ref}.

Valence band measurements were deduced with the aid of X-ray photoelectron spectroscopy (XPS), which was conducted with a Thermo spectroscope, model ESCALAB 250Xi, using a Al Kα monochromator (1486.7 eV) as an excitation source at a working pressure of $<10-8$ mBar.

Electrophoretic light scattering (ELS) using a Zetasizer Nano ZS (Malvern) was used to deduce surface charge measurements.

4.3.2. Photocatalytic Experiment

The degradation setup comprised a UV lamp (ENF-240C/FE, Spectronics Corporation Westbury, NY, USA) which provided UV light of wavelength 365 nm. For all experiments, 300 mL (10–50 mg/L) of diazinon concentration was illuminated in the presence of 0.1–2 g/L of the photocatalyst at a certain pH (2–10). The initial pH of the solution was adjusted with 2M HCl and 2M NaOH. All runs were performed in triplicate under ambient conditions for 1 h The suspension solution in the photoreactor was kept at room temperature and was continuously stirred. The photocatalyst suspension was equilibrated in the dark for half an hour. Once adsorption–desorption equilibrium was reached, the suspensions were irradiated with UV light. Approximately 3 mL was sampled at 5 min intervals for 30 min. The diazinon concentration was measured using a Shimadzu UV-2450 UV–Vis spectrophotometer at a wavelength of 295 nm. The percentage removal was computed using Equation (12).

$$\% \text{ diazinon removal} = \left(1 - \frac{[\text{diazinon}]}{[\text{diazinon}]_0}\right) \times 100 \quad (12)$$

where $[\text{diazinon}]_0$ = initial diazinon concentration and $[\text{diaiznon}]$ = final diazinon concentration.

The reaction kinetics of diazinon photodegradation were investigated and the first-order model fit the results and the plot based on calculated $\ln([\text{diazinon}]/[\text{diazinon}]_0)$ against duration of reaction was obtained.

$$\ln([\text{diazinon}]/[\text{diazinon}]_0) = \ln[\text{diazinon}]_0 - kt \quad (13)$$

where k is defined as the reaction constant and t represents the reaction time.

The reaction rate was extrapolated from the slope of the plot defined above calculated from Equation (13).

5. Conclusions

In this work, the application of MIL/BP composites for the photodegradation of diazinon was investigated. The 4%BpMIL showed the best removal efficiency compared to the other nanocomposites and as such was selected as the optimum photocatalyst for the subsequent investigation of the other degradation parameters. The greatest degradation

efficiency was observed at neutral pH. As the quantity of the photocatalyst was increased to 0.5 g/L, the effectual photodegradation efficiency was enhanced, however, it decreased when the loading of the photocatalyst was increased to 2 g/L. The kinetic studies revealed that the degradation followed pseudo-first-order kinetics.

Author Contributions: Conceptualization, L.N.D.; methodology, P.V.H. and L.N.D.; formal analysis, P.V.H. and L.N.D.; investigation, P.V.H.; resources, L.N.D..; data curation, P.V.H.; writing—original draft preparation, P.V.H.; writing—review and editing, L.N.D.; supervision, L.N.D.; project administration, L.N.D.; funding acquisition, L.N.D. All authors have read and agreed to the published version of the manuscript.

Funding: This research was funded by the University of Johannesburg (URC) and Faculty of Science (FRC), National Research Foundation (TTK180424323810), Centre for Nanomaterials Science Research (CNSR) and Nanomaterials Innovation Centre (NIC).

Data Availability Statement: The data presented in this study are available on request from corresponding author. The data are not publicly available due to ethical reasons.

Conflicts of Interest: The authors declare no conflict of interest.

References

1. Jonidi-Jafari, A.; Shirzad-Siboni, M.; Yang, J.; Naimi-Joubani, M.; Farrokhi, M. Photocatalytic degradation of diazinon with illuminated ZnO-TiO_2 composite. *J. Taiwan Inst. Chem. Eng.* **2015**, *50*, 100–107. [CrossRef]
2. Survey of Pesticide Wastes in South Africa and Review of Treatment Options, Water Research Commision. 2003. Available online: https://www.wrc.org.za (accessed on 7 March 2020).
3. Katsumata, H.; Matsumoto, T.; Kaneco, S.; Suzuki, T.; Ohta, K. Preconcentration of diazinon using multiwalled carbon nanotubes as solid-phase extraction adsorbents. *J. Microc.* **2008**, *50*, 82–86. [CrossRef]
4. Zhang, Y.; Hou, Y.; Chen, F.; Xiao, Z.; Zhang, J.; Hu, X. The degradation of chlorpyrifos and diazinon in aqueous solution by ultrasonic irradiation: Effect of parameters and degradation pathway. *J. Chemosphere* **2011**, *82*, 1109–1115. [CrossRef] [PubMed]
5. Jonidi-Jafari, A.; Gholami, M.; Farzadkia, M.; Esrafili, A.; Shirzad-Siboni, M. Application of Ni-doped ZnO nanorods for degradation of diazinon: Kinetics and by-products. *J. Sep. Sci. Technol.* **2017**, *52*, 2395–2406. [CrossRef]
6. Molla, A.I.; Furukawa, M.; Tateishi, I.; Katsumata, H. Mineralization of Diazinon with nanosized-photocatalyst TiO_2 in water under sunlight irradiation: Optimization of degradation conditions and reaction pathway. *J. Environ. Technol.* **2019**, *10*, 1–10. [CrossRef] [PubMed]
7. Dong, H.; Zeng, G.; Tang, L.; Fan, C.; Zhang, C.; He, X.; He, Y. An overview on limitations of TiO_2-based particles for photocatalytic degradation of organic pollutants and the corresponding countermeasures. *J. Water. Res.* **2009**, *79*, 128–146. [CrossRef]
8. Ibhadon, A.; Fitzpatrick, P. Heterogeneous Photocatalysis: Recent Advances and Applications. *J. Catal.* **2013**, *3*, 189–218. [CrossRef]
9. Marschall, R. Semiconductor composites: Strategies for enhancing charge carrier separation to improve photocatalytic activity. *J. Adv. Funct. Mater.* **2014**, *24*, 2421–2440. [CrossRef]
10. Tang, K.; Yin, W.; Zhang, L.; Wen, B.; Zhang, D.; Liu, L.; Lau, W. Spatial separation of photo-generated electron-hole pairs in BiOBr/BiOI bilayer to facilitate water splitting. *J. Sci. Rep.* **2016**, *6*, e0032764. [CrossRef]
11. Hendon, C. Hybrid Semiconductors: Design Rules and Material Applications. Ph.D. Thesis, University of Bath, Bath, UK, 2015.
12. Devic, T.; Serre, C. High valence 3p and transition metal based MOFs. *J. Chem. Soc. Rev.* **2014**, *43*, 6097–6115. [CrossRef]
13. Zhou, H.; Kitagawa, S. Metal–Organic Frameworks (MOFs). *J. Chem. Soc. Rev.* **2014**, *43*, 5415–5418. [CrossRef] [PubMed]
14. McGuire, C.; Forgan, R. The surface chemistry of metal-organic frameworks. *J. Chem. Commun.* **2015**, *51*, 5199–5217. [CrossRef]
15. Yuan, X.; Wang, H.; Wu, Y.; Zeng, G. One-pot self-assembly and photoreduction synthesis of silver nanoparticle-decorated reduced graphene oxide/MIL-125 (Ti) photocatalyst with improved visible light photocatalytic activity. *J. App. Org. Chem.* **2016**, *30*, 289–296. [CrossRef]
16. Wang, H.; Yaun, X.; Wu, Y.; Zeng, G.; Chen, X.; Li, L. Synthesis and applications of novel graphitic carbon nitride/metal-organic frameworks mesoporous photocatalyst for dyes removal. *J. Appl. Catal. B Environ.* **2015**, *174–175*, 445–454. [CrossRef]
17. Yang, Z.; Ding, J.; Feng, J.; He, C.; Li, Y.; Tong, X.; Niu, X.; Zhang, H. Preparation of $BiVO_4$/MIL-125(Ti) composite for enhanced visible-light driven photocatalytic activity for dye degradation. *J. Appl. Organomet. Chem.* **2018**, *32*, 1–10. [CrossRef]
18. Wang, H.; Yaun, X.; Wu, Y.; Zeng, G.; Chen, X.; Leng, L.; Wu, Z.; Jiang, L.; Li, H. Facile synthesis of amino-functionalized titanium metal-organic frameworks and their superior visible-light photocatalytic activity for Cr(VI) reduction. *J. Hazard. Mater.* **2015**, *286*, 187–194. [CrossRef] [PubMed]
19. Zhu, M.; Osakada, Y.; Kim, S.; Fujitsuka, M.; Majima, T. Black phosphorus: A promising two dimensional visible and near-infrared-activated photocatalyst for hydrogen evolution. *J. Appl. Catal. B Environ.* **2017**, *217*, 285–292. [CrossRef]
20. Liu, H.; Du, Y.; Deng, Y.; Ye, P. Semiconducting black phosphorus: Synthesis, transport properties and electronic applications. *J. Chem. Soc. Rev.* **2015**, *44*, 2732–2743. [CrossRef] [PubMed]

21. Zhang, C.; Qiu, L.; Ke, F.; Zhu, Y.; Yaun, Y.; Xu, G.; Jiang, X. A novel magnetic recyclable photocatalyst based on a core-shell metal-organic framework Fe_3O_4@MIL-100(Fe) for the decolorization of methylene blue dye. *J. Mater. Chem. A* **2013**, *45*, 14329–14334. [CrossRef]
22. Jin, M.; Qian, X.; Gao, J.; Chen, J.; Hensley, D.; Ho, H.; Percoco, R.; Ritzi, C.; Yue, Y. Solvent-Free Synthesis of CuO/HKUST-1 composite and its photocatalytic application. *Inorg. Chem.* **2019**, *58*, 8332–8338. [CrossRef]
23. Hlophe, P.; Dlamini, L. Synthesis of semi-conductor-like black phosphorous as a composite for visible light-driven photocatalysis. *J. RSC Adv.* **2019**, *9*, 37321–37330. [CrossRef]
24. Kouloumbos, V.; Tsipi, D.; Hiskia, A.; Nikolic, D.; Breemen, R. Identification of photocatalytic degradation products of diazinon in TiO_2 aqueous suspensions using GC/MS/MS and LC/MS with quadrupole time-of-flight mass spectrometry. *J.Am. Soc. Mass Spectrom.* **2003**, *14*, 803–817. [CrossRef]
25. Shemer, H.; Linden, K. Degradation and by-product formation of diazinon in water during UV and UV/H_2O_2 treatment. *J. Hazard. Mater.* **2006**, *136*, 553–559. [CrossRef] [PubMed]
26. Hlophe, P.; Dlamini, L.; Mahlalela, L. A composite of platelet-like orientated BiVO 4 fused with MIL-125 (Ti): Synthesis and characterization. *J. Sci. Rep.* **2019**, *9*, 1–12.